Electronic structure of ScN determined using optical spectroscopy, photoemission, and *ab initio* calculations

D. Gall,[1] M. Städele,[2] K. Järrendahl,[3] I. Petrov,[1] P. Desjardins,[1] R. T. Haasch,[1] T.-Y. Lee,[1] and J. E. Greene[1,3]
[1]*Materials Science Department and the Frederick Seitz Materials Research Laboratory, University of Illinois, 104 South Goodwin, Urbana, Illinois 61801*
[2]*Beckman Institute, University of Illinois, 405 North Mathews Avenue, Urbana, Illinois 61801*
[3]*Department of Physics, Linköping University, SE-581 83 Linköping, Sweden*
(Received 3 April 2000; published 13 March 2001)

Experimental and *ab initio* computational methods are employed to conclusively show that ScN is a semiconductor rather than a semimetal; i.e., there is a gap between the N $2p$ and the Sc $3d$ bands. Previous experimental investigators reported, in agreement with band structure calculations showing a band overlap of 0.2 eV, that ScN is a semimetal while others concluded that it is a semiconductor with a band gap larger than 2 eV. We have grown high quality, single crystalline ScN layers on MgO(001) and on TiN(001) buffer layers on MgO(001) by ultrahigh vacuum reactive magnetron sputter deposition. ScN optical properties were determined by transmission, reflection, and spectroscopic ellipsometry while *in-situ* x-ray and ultraviolet valence band photoelectron spectroscopy were used to determine the density of states (DOS) below the Fermi level. The measured DOS exhibits peaks at 3.8 and 5.2 eV stemming from the N $2p$ bands and at 15.3 eV due to the N $2s$ bands. The imaginary part of the measured dielectric function ε_2 consists of two primary features due to direct X- and Γ-point transitions at photon energies of 2.7 and 3.8 eV, respectively. For comparison, the ScN band structure was calculated using an *ab initio* Kohn–Sham approach which treats the exchange interactions exactly within density-functional theory. Calculated DOS and the complex dielectric function are in good agreement with our ScN valence-band photoelectron spectra and measured optical properties, respectively. We conclude, combining experimental and computational results, that ScN is a semiconductor with an indirect $\Gamma - X$ bandgap of 1.3 ± 0.3 eV and a direct X-point gap of 2.4 ± 0.3 eV.

DOI: 10.1103/PhysRevB.63.125119 PACS number(s): 71.20.Nr, 71.20.Be, 71.15.Mb

I. INTRODUCTION

ScN is a B-1 NaCl-structure III–V compound with an electronic structure characterized by the Fermi level being located exactly between the N $2p$ and Sc $3d$ bands. However, there has been a longstanding debate in the literature as to whether there is band overlap or a gap in the ScN density of states (DOS); that is, whether ScN is a semimetal or a semiconductor. Self-consistent augmented-plane-wave (APW) band structure calculations by Neckel *et al.*[1,2] and Monnier *et al.*,[3] employing the heuristic Xα and the local-density-approximation (LDA) for the exchange-correlation potential, respectively, predict metallic conductivity due to a small, 0.01–0.21 eV, overlap of valence bands at the Γ point with the conduction bands at the X point. The direct transitions between the N $2p$ and the Sc $3d$ bands have been predicted to be 0.8 and 2.7 eV at the X and Γ points, respectively. However, the reliability of the relative values of the band-edge energies in these results has been questioned by Schwarz[4] in a review of bandstructure calculations for transition-metal (TM) nitrides and carbides. In addition, it is well known[5] that LDA seriously underestimates bandgaps (typically by a few eV). This suggests that the actual ScN band gap may be considerably larger than the values obtained by the above-mentioned calculations.

Johansson[6] compared APW $X\alpha$ band structure calculations for various NaCl-structure TM nitrides and carbides with angle-resolved photoelectron spectroscopy data and found systematic differences at high symmetry points in the Brillouin zone. In the case of TiN,[7] the compound most similar to ScN, the energy of the Δ_5 valence band at the Γ point was predicted 1 eV too high and the $\Delta_{2'}$ conduction band at the X point was 1 eV too low. For the ScN band structure calculations, published in the same paper with those for TiN,[1] these two points define the valence and conduction band overlap which means that, assuming a similar error in the ScN calculations, ScN could have a band gap of up to approximately 2 eV.

In contradiction to previous theoretical results predicting metallic conductivity, there are several experimental reports[8–15] showing optical absorption measurements with a rather steep absorption edge above 2 eV, indicating that ScN is a semiconductor. Sclar[8,9] prepared pressed-powder $ScN_{0.9}$ and proposed, although the absorption spectra were not conclusive, an optical energy gap of 2.6 eV. Dismukes *et al.*[10–12] reported the growth of $ScN_{0.98}$ on α-$Al_2O_3(1\bar{1}02)$ by chemical vapor deposition (CVD) from NH_3 and halides produced by the reaction of HCl, HBr, or HI with Sc. Hall measurements showed a donor concentration of $10^{20}-10^{21}\,cm^{-3}$ which the authors assumed to arise from incorporated halogen impurities. Nevertheless, optical absorption measurements yielded, after subtraction of free carrier effects, an estimated optical band gap of 2.1 eV. Similar results were obtained by Kaldis *et al.*[13] for $ScN_{0.93-0.98}$ grown by reactive evaporation.

Moustakas *et al.*[14] reported the growth of stoichiometric polycrystalline ScN films by electron cyclotron resonance plasma-assisted molecular beam epitaxy (ECR–MBE) on

$Al_2O_3(0001)$ substrates and measured a fundamental absorption edge at 2.1 eV. *In-situ* x-ray and ultraviolet valence band spectroscopy (XPS and UPS) measurements were carried out by Porte[16] on ScN films deposited by reactive sputter deposition on Ta foil. He found the valence bands to be 1.5–2 eV lower than the position predicted by calculations from Ref. 1, thus concluding that ScN is semiconducting with a band gap of 1.5–2 eV. We reported the growth of polycrystalline $ScN_{0.98}$ films on MgO(001) at 750 °C by reactive magnetron sputtering.[15] The temperature dependent resistivity of these layers exhibited semiconductor behavior and optical absorption yielded a direct transition at 2.37 eV.

There is, however, also an experimental report supporting the APW LDA bandstructure calculations. Travaglini *et al.*[17] measured the optical reflectivity of bulk single crystal $ScN_{0.99}$ samples, obtained by nitriding Sc at 2000 °C and annealing at 2180 °C, over four decades of photon energy from 1 meV to 12 eV, and used a Kramers–Kronig analysis to derive the dielectric function. The observed absorption peaks at 0.8 and 2.6 eV were related to direct transitions at the *X* and Γ point, respectively. They also reported features below 0.2 eV which they related to intraband transitions near the bottom of the conduction band at the *X* point or near the top of the valence band at the Γ point and thus concluded that ScN is a semimetal with a band overlap of 0.2 eV.

All experimental results published on ScN at least agree that there is an abrupt absorption edge somewhere between 2 and 2.6 eV due to a direct interband transition. However, there has been no agreement upon whether ScN is semiconducting or semimetallic. We believe that a primary reason for the disparity is the difficulty in obtaining single crystalline, stoichiometric, high purity ScN. In addition, the only available band structure data were derived from calculations based on LDA or $X\alpha$, which are not well suited for accurate band-gap predictions.

Recently, we reported the growth of stoichiometric, epitaxial ScN(001) layers on MgO(001) and on TiN(001)/MgO(001) by ultrahigh vacuum (UHV) reactive magnetron sputter deposition.[18,19] The layers were shown, using a combination of techniques including high-resolution x-ray diffraction (HR–XRD), transmission electron microscopy (TEM), cross-sectional TEM (XTEM), x-ray reflectivity, Rutherford back scattering (RBS), and x-ray photoelectron spectroscopy (XPS), to be stoichiometric high-quality single crystals. The ScN samples used in the experiments reported here were grown in the same apparatus and exhibit the same structural quality and stoichiometry as those described in Refs. 18 and 19.

In this paper, we report optical properties and *in-situ* valence-band photoelectron spectra for epitaxial ScN(001) grown on both MgO(001) and on TiN(001) buffer layers on MgO(001). Optical absorption below the direct transition energy was measured to be $\simeq 6\times 10^3\ cm^{-1}$. This is a factor of 2–10 times lower than earlier experimental reports[11,17] and is another indicator of the high quality of the ScN layers used in this investigation.

The experimental results are correlated with *ab initio* electronic structure calculations which predict an indirect band gap of 1.6 eV. In order to circumvent the well-known difficulties associated with standard LDA bandstructure calculations, we utilized a recently developed Kohn–Sham density functional method[20,21] (termed EXX) that treats exchange interactions exactly and therefore represents a systematic step beyond the commonly used density-functional methods. The EXX scheme has been shown to yield very accurate bandgaps, typically within 0.2 eV, for a wide variety of semiconductors.[21] Calculated DOS and the complex dielectric function for ScN are in good agreement with our valence-band photoelectron spectra and optical properties, respectively. Both the measured DOS and the optical properties can only be explained with an electronic structure which exhibits a bandgap and we conclude, using a combination of experiment and calculation, that ScN is an indirect semiconductor with a fundamental gap of 1.3 ± 0.3 eV.

II. EXPERIMENTAL PROCEDURE

The ScN layers were grown in a two-chamber turbomolecular-pumped UHV deposition system consisting of a sample introduction chamber and a three-target magnetron growth chamber with a base pressure of 1×10^{-9} Torr (1.3×10^{-7} Pa). Two 5-cm-diameter water-cooled sputtering targets were used; the Ti target is 99.999% pure and Sc is 99.99% with the only contaminant detectable by Rutherford backscattering spectroscopy (RBS) being 0.01 at% Ta, the normal impurity in Sc. Both the TiN buffer layers and the ScN overlayers were deposited in pure N_2 (99.999%) at 5 mTorr (0.7 Pa). Current-regulated dc power supplies provided a discharge current of 0.5 A at 485 V for growth of TiN and 1.5 A at 312 V for ScN. The resulting deposition rates, with a target-to-substrate separation of 15 cm, were 132 and 186 nm h^{-1}, respectively, in the fully target-nitrided regime.

The substrates were polished $10\times 10\times 0.5$ mm MgO(001) wafers which were cleaned, degreased, and degassed according to the procedure described in Ref. 22. The TiN buffer layers were deposited at 750 °C, the temperature raised to 800 °C, and the ScN overlayers grown without breaking vacuum. ScN layers for optical transmission experiments were grown directly on MgO(001) in a magnetically unbalanced mode as described in Ref. 18. This required a slightly lower growth temperature, 750 °C, in order to avoid ScN/MgO interfacial reactions.

Film microstructure and texture were investigated using HR–XRD and XRD pole figure analyses. A Philips MRD diffractometer with $CuK_{\alpha 1}$ radiation ($\lambda = 0.1540597$ nm) from a four-crystal Ge(220) monochromator, which provided an angular divergence of ≃12 arc s with a wavelength spread $\Delta\lambda/\lambda \simeq 7\times 10^{-5}$ was used to collect ω and ω-2θ scans with a detector acceptance angle of ≃2°. The microchemistry of as-deposited layers was examined using both RBS and XPS. The RBS probe beam consisted of 2 MeV He^+ ions incident at an angle of 22.5° relative to the sample surface normal with the detector set at a 150° scattering angle. XPS measurements were carried out in a Physical Electronics PHI 5400 spectrometer equipped with a MgK_α x-ray source and a hemispherical detector. Air exposed samples were sputter

etched using a low-angle (~20°), 0.5 keV Ar^+ beam before acquiring XPS data.

Optical transmission and reflection spectra were obtained between 300 and 2000 nm using a Perkin-Elmer Lambda 9 spectrophotometer with an integrating sphere for light collection. Measured reflectivity from an undoped single crystal Si(001) wafer was used to calibrate spectral intensity distributions. ScN optical properties were also probed using a variable angle of incidence spectroscopic ellipsometer (VASE) with photon energies between 1.24 and 5.0 eV and the beam incident at 60°, 65°, and 70°. A unique solution for the complex dielectric function of ScN was obtained from VASE data using the multiple sample analysis described in Appendix I.

The ScN density of states (DOS) below the Fermi level was determined by *in-situ* valence band x-ray and ultraviolet photoelectron spectroscopy (XPS and UPS). For this purpose, a UHV deposition system, similar to the one described above, was attached, via a sample transfer chamber, to a Physical Electronics PHI 5400 photoelectron spectrometer. Epitaxial ScN(001) layers, 40 nm thick, were grown on MgO(001) substrates by reactive magnetron sputter deposition following the above described procedure, and transferred in UHV to the analysis chamber where He I (21.2 eV), He II (40.8 eV), and XPS spectra were acquired. The UPS source was incident at an angle of 50° while photons from the monochromatized Al K_α (1486.6 eV) x-ray source were incident at 45° to the sample surface normal. The spherical sector analyzer was operated in a constant pass energy (8.95 and 17.9 eV) mode, resulting in a resolution of 0.13 and 0.27 eV for UPS and XPS, respectively. Detector acceptance angles were 22°, 14°, and 3° measured at 9, 25, and 1010 eV for He I, He II, and Al K_α spectra, respectively. The energy scale was calibrated using clean Au and Cu samples; the Fermi level was set to 0 eV binding energy; and the Au $4f_{7/2}$ (width=0.81 eV) and Cu $2p_{3/2}$ (width=1.01 eV) peaks were set to 84.0 and 932.7 eV, respectively.

III. COMPUTATIONAL METHOD

In this section, we briefly outline the EXX formalism that has been used for the present ScN band-structure calculations. EXX has been shown to predict semiconductor band gaps much more accurately than the standard local density approximation[21] and is described in detail in Ref. 21.

The EXX scheme relies on the solution of the Kohn–Sham equations[23] of density-functional theory,

$$\left[-\frac{\hbar^2\nabla^2}{2m}+V_{\mathrm{KS}}(\mathbf{r})\right]\varphi_{n\mathbf{k}}(\mathbf{r})=\varepsilon_{n\mathbf{k}}\varphi_{n\mathbf{k}}(\mathbf{r}) \tag{1}$$

for the single-particle Bloch states $\varphi_{n\mathbf{k}}$ with band index n, wave vector $\mathbf{k}$, and eigenenergy $\varepsilon_{n\mathbf{k}}$. The total local Kohn–Sham potential is approximated as

$$V_{\mathrm{KS}}(\mathbf{r})=V_{\mathrm{ext}}(\mathbf{r})+V_{\mathrm{H}}(\mathbf{r})+V_x(\mathbf{r})+V_c^{\mathrm{LDA}}(\mathbf{r}). \tag{2}$$

V_{ext} in Eq. (2) is the external potential due to the ion cores, V_{H} the Hartree potential, V_x the exact exchange potential, and V_c^{LDA} is the correlation potential obtained by LDA. The characteristic feature of the EXX method is calculation of the exact exchange potential via the explicit expression

$$V_x(\mathbf{G})=\sum_{\mathbf{G}'\neq 0}\lfloor E(\mathbf{G}')+E^*(-\mathbf{G}')\rfloor\tilde{\chi}_0^{-1}(\mathbf{G},\mathbf{G}'),$$
$$E(\mathbf{G})=\frac{2}{\Omega}\sum_{v\mathbf{c}\mathbf{k}}\frac{\langle v\mathbf{k}|\hat{V}_x^{\mathrm{NL}}|c\mathbf{k}\rangle\langle c\mathbf{k}|e^{-i\mathbf{G}r}|v\mathbf{k}\rangle}{\varepsilon_{v\mathbf{k}}-\varepsilon_{c\mathbf{k}}}, \tag{3}$$

where $\mathbf{G}$ and $\mathbf{G}'$ are reciprocal lattice vectors, $\tilde{\chi}_0^{-1}$ is the effective inverse of the independent-particle polarizability in the Fourier-space representation (excluding $\mathbf{G}$, $\mathbf{G}'=0$), and $\hat{V}_x^{\mathrm{NL}}$ denotes a nonlocal operator which has the same form as the Hartree–Fock exchange operator, but is constructed of Kohn–Sham (rather than Hartree–Fock) orbitals $\varphi_{n\mathbf{k}}$.

The EXX scheme has been implemented using a plane-wave basis with a kinetic energy cutoff of 45 Ry for the wave functions and 32 Ry for $\tilde{\chi}_0$. Scalar-relativistic exact exchange pseudopotentials[24] with cutoff radii $r_s=r_p=r_d=1.7$ a.u. for N and $r_s=2.65$, $r_p=2.85$, and $r_d=2.65$ a.u. for Sc were employed and ten special k points were used for the Brillouin-zone summations. For the summations over conduction bands in Eq. (3), all conduction states included in the Hamiltonian have been used. These parameters guarantee that bandgaps are converged within ≃0.1 eV.

IV. RESULTS

N/Sc ratios in as-deposited ScN layers were measured by RBS and the spectra analyzed using the RUMP simulation program.[25] The results show that the films are stoichiometric with N/Sc=1.00±0.02. An additional measure of film composition was provided by XPS. In this case, N/Sc was determined by removing the background using an integrating algorithm, fitting the N 1*s* and Sc 2*p* peaks with asymmetric Gaussian–Lorentzian curves, and using sensitivity factors from Ref. 26. The results, N/Sc=1.00±0.05, are in excellent agreement with the RBS data. No impurities, other than the 0.01 at% Ta (in the form of TaN) from the Sc target, were detected by either RBS or XPS.

A typical HR-XRD ω-2θ scan through the MgO substrate 002 Bragg peak is presented in Fig. 1 for a 62-nm-thick ScN film deposited on a 220-nm-thick TiN buffer layer. The angular separation between the substrate and the layer peaks, $\Delta\omega=1.54$, yields an out-of-plane lattice constant $a_\perp=0.4517$ nm. This value is 0.3% larger than the bulk lattice constant, 0.4501 nm, showing that the film exhibits a slight in-plane compression due to differential thermal contraction during cooling from the deposition temperature.[19] The ScN diffraction peak is symmetric with a full-width at half-maximum intensity (FWHM) $\Gamma_{\omega-2\theta}=0.47°$. The 002 ω rocking curve shown in the inset is also symmetric with $\Gamma_\omega=1.10°$. Using the measured ω-2θ and ω FWHM values, we calculate in-plane and out-of-plane x-ray coherence lengths of 12 and 20 nm, respectively,[27] indicating good crystalline quality, XRD {111} and {002} pole figures (not shown), together with TEM and XTEM analyses, establish that the ScN layers are single crystals which grow with a cube-on-cube

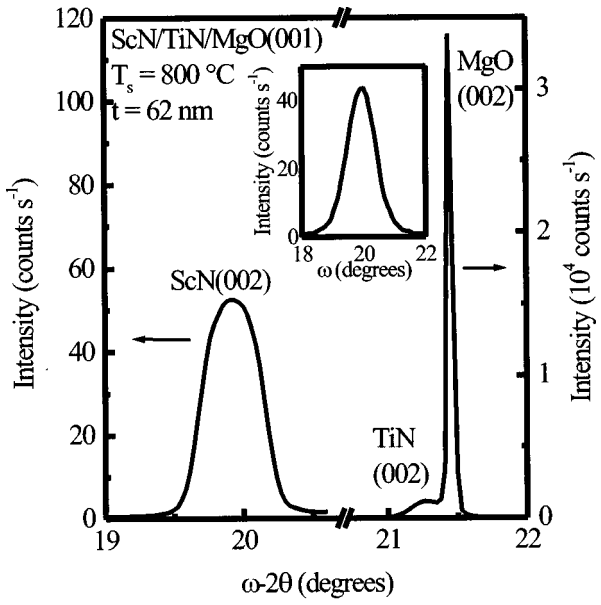

FIG. 1. High-resolution XRD ω-2θ scan and 002 ω rocking curve (inset) from a 62-nm-thick ScN film deposited on a 220-nm-thick TiN buffer layer on MgO(001).

epitaxial relationship: $(001)_{ScN}\|(001)_{TiN}\|(001)_{MgO}$ and $[100]_{ScN}\|[100]_{TiN}\|[100]_{MgO}$.

Figure 2 shows the EXX band structure of ScN, plotted along high symmetry directions in the Brillouin zone. The N 2*s* band has a width of 1.8 eV and is 13.1–14.9 eV below the zero of the energy scale which is set to the top of the valence band. The N 2*p* bands, separated by 7.8 eV from the N 2*s* band, have a width of 5.3 eV and their maximum and minimum are at the Γ and *L* point, respectively. The minimum in the Sc 3*d* conduction bands occurs at the *X* point, 1.6 eV above the valence band maximum at Γ. These results indicate that ScN is an indirect gap semiconductor with a Γ to *X* band gap of 1.6 eV. The direct gaps at the *X* and Γ points, from $X_{5'}$ to X_3 and Γ_{15} to $\Gamma_{25'}$, are 2.9 and 4.7 eV, respectively.

We determine the ScN optical absorption spectrum from transmission and reflection experiments. For this purpose, epitaxial 173, 345, and 518-nm-thick ScN layers were grown

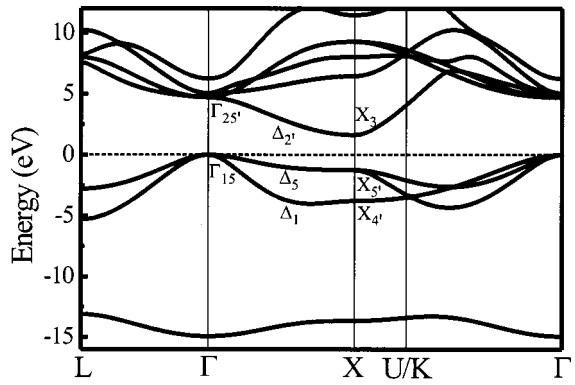

FIG. 2. ScN EXX bandstructure calculation along high symmetry directions in the Brillouin zone.

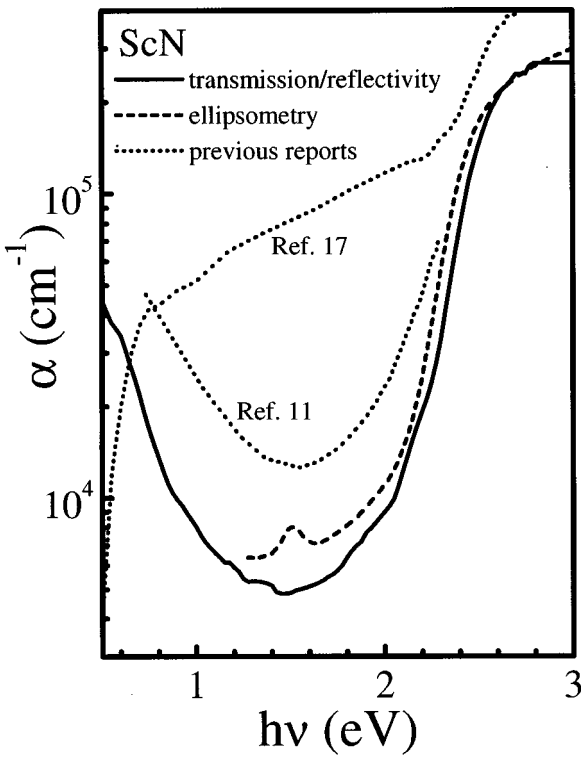

FIG. 3. Comparison of ScN optical absorption spectra obtained from transmission/reflection measurements on ScN(001)/MgO(001) layers, from spectroscopic ellipsometry analyses of ScN/TiN/MgO(001) layers, and from previous reflectivity measurements carried out on bulk single crystal ScN (Ref. 17) and ScN layers grown by halide CVD (Ref. 11).

directly on transparent MgO(001) substrates. The absorption coefficient α as a function of wavelength λ was then obtained from the following expression, using measured transmittance $T(\lambda)$ and reflectance $R(\lambda)$ data,

$$\alpha(\lambda)=\frac{1}{t}\ln\left(\frac{1-R(\lambda)}{T(\lambda)}\right). \tag{4}$$

ScN layers with different thicknesses *t*, as measured by XTEM, resulted in identical values of α. Figure 3 shows a plot of α vs photon energy $h\nu$. For comparison, we also plot the results obtained from ellipsometry measurements of ScN layers grown on TiN/MgO, as described below, as well as previously reported α vs $h\nu$ curves obtained from reflectivity measurements on bulk single crystal ScN[17] and polycrystalline ScN layers grown by halide CVD.[11]

The present results show that ScN is relatively transparent ($\alpha<10^4\ \mathrm{cm}^{-1}$) between $\simeq$1 eV and 2.3 eV. Below 1 eV, absorption due to conduction electrons becomes significant and above 2.3 eV the nature of the spectrum is determined by interband transitions. Figure 3 also shows that the ellipsometry data agree very well with our transmission/reflection results except that the onset of interband transitions occurs at a slightly lower (0.05 eV) energy in the former. This apparent shift, caused by the Moss–Burstein effect,[28] is due to a change in free carrier density which is determined by the

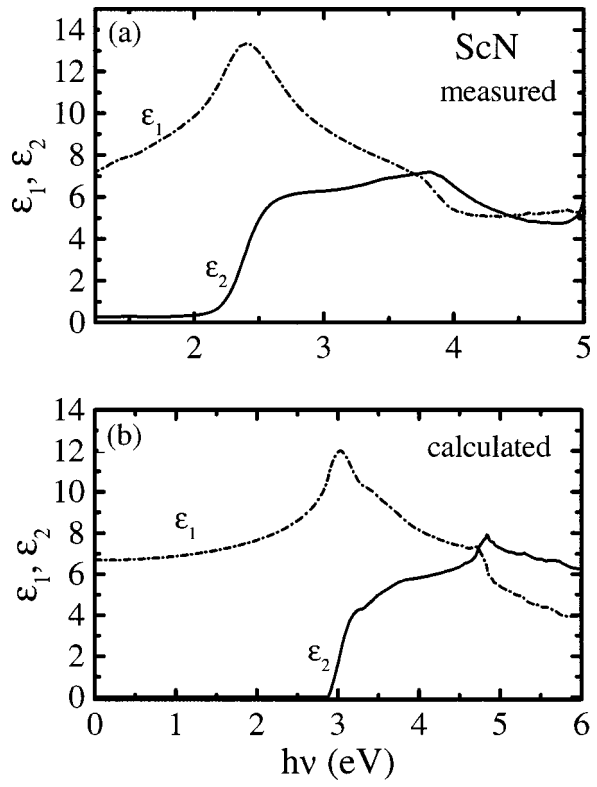

FIG. 4. ScN dielectric function, $\varepsilon_{\mathrm{ScN}}=\varepsilon_1+i\varepsilon_2$, obtained from (a) spectroscopic ellipsometry multiple-sample analyses and from (b) *ab initio* EXX calculations.

N-vacancy concentration and thus by the specific growth conditions, which are different for layers grown on MgO (for transmission/reflectivity measurements) and TiN (for ellipsometry measurements). The logarithmic scale also reveals a small artifact at 1.5 eV due to surface effects which result in relatively large uncertainties in α values determined from ellipsometry measurements over wavelength ranges where the film is only weakly absorbing. This feature is absent in the spectra from the transmission/reflection measurements which are carried out on films with thicknesses which are up to a factor of seven larger, rendering surface effects negligible.

The absorption coefficients reported by Dismukes *et al.*[11] and Travaglini *et al.*[17] (also plotted in Fig. 3) exhibit a sharp increase between 2 and 2.7 eV, consistent with our results. However, the absorption of our films in the spectral region below 2.5 eV is considerably lower, by factors of 2 and 10, respectively. This indicates that the samples used in the previous studies either had lower purity, higher defect densities, and/or were unstoichiometric. The presence of significant surface oxidation and roughness may also have influenced the results of the previous studies.

Figure 4(a) shows the real and imaginary parts of the ScN dielectric function, $\varepsilon_{\mathrm{ScN}}=\varepsilon_1+i\varepsilon_2$, obtained from analyses of the ellipsometry data. For this purpose, epitaxial ScN(001) layers with thicknesses of 70 and 79 nm, as determined from XTEM measurements, were grown on optically opaque TiN(001) buffer layers on MgO(001). Spectroscopic ellipsometry data from the samples were compared to data calculated from an ambient/overlayer/film/substrate model. The optical properties of the substrate (the opaque TiN buffer layer) were obtained from spectroscopic ellipsometry measurements of a TiN(001) layer grown under the same conditions, but without the ScN. Surface oxides and microscopic surface roughness influence the measurements and were thus included in the model as an ''overlayer'' modeled using the Bruggeman effective medium-approximation[29] in which an effective dielectric constant $\varepsilon_{\mathrm{eff}}$ is calculated from a mixture of two materials (with dielectric functions ε_A and ε_B) according to

$$f\frac{\varepsilon_A-\varepsilon_{\mathrm{eff}}}{\varepsilon_A+2\varepsilon_{\mathrm{eff}}}+(1-f)\frac{\varepsilon_B-\varepsilon_{\mathrm{eff}}}{\varepsilon_B+2\varepsilon_{\mathrm{eff}}}=0, \tag{5}$$

where f is the fraction of material A. In this case, A and B are the ambient ($\varepsilon=1$) and ScN with f assumed to be 0.5. This approach has proven to be a good approximation for surface roughness effects.[29]

Surface oxides and roughness should, in principle, be treated separately but since the effects are similar,[30] only one overlayer was introduced to reduce the number of parameters in the model. Thus the unknown parameters are only the frequency-dependent ScN optical properties $\varepsilon_{\mathrm{ScN}}(h\nu)$, the optical layer thickness d_{ScN} and the overlayer thickness d_{ol}. In order to simultaneously obtain $\varepsilon_{\mathrm{ScN}}(h\nu)$, d_{ScN}, and d_{ol}, multiple-sample analysis[31,32] was used in which measurements from two samples, at three different beam incidence angles each, were simultaneously fit using coupled optical properties $\varepsilon_{\mathrm{ScN}}(h\nu)$. In the first ScN sample, the sum ($d_{\mathrm{ScN}}+d_{\mathrm{ol}}$) was found to be 66 nm with $d_{\mathrm{ol}}=3.8$ nm while in the second sample ($d_{\mathrm{ScN}}+d_{\mathrm{ol}}$)$=79$ nm with $d_{\mathrm{ol}}=4.6$ nm. These film thicknesses are in good agreement with XTEM observations, $t=70$ and 79 nm. The thickness of the overlayer of the second sample was determined by x-ray reflectivity to be 4.9 nm,[19] also in agreement with the optical results, $d_{\mathrm{ol}}=4.6$ nm.

The dielectric function spectra, obtained using the above procedure, are plotted in Fig. 4(a) over the photon energy range from 1.24–5 eV. The spectra exhibit no indication of intraband transitions, consistent with our transmission/reflection results which show that free-electron absorption is observed only below $\simeq 1$ eV and thus outside the wavelength range accessible in these measurements. ε_2 is small for $h\nu<2$ eV. Hence, ScN is only weakly absorbing in this energy range. Above 2 eV, $\varepsilon_2(h\nu)$ increases rapidly up to 6.1 indicating a resonance peak with a maximum near 2.7 eV. There is a second resonance at 3.8 eV where $\varepsilon_2=7.2$. The ε_1 spectra follows the shape expected from basic oscillator theory.[33] It increases monotonically up to a maximum of 13.3 at 2.4 eV, indicating the onset for interband transitions and corresponding to a Lorentz oscillator with a resonance frequency of $\simeq 2.7$ eV. ε_1 decreases at higher energies and has the steepest slope near the second resonance at 3.8 eV.

The dielectric function spectra in Fig. 4(a) are similar to reported curves obtained from reflectivity measurements from bulk ScN.[17] The positions of the prominent features are the same, but the absolute values are quite different. In fact, the ε_1 values obtained in the present experiments are consis-

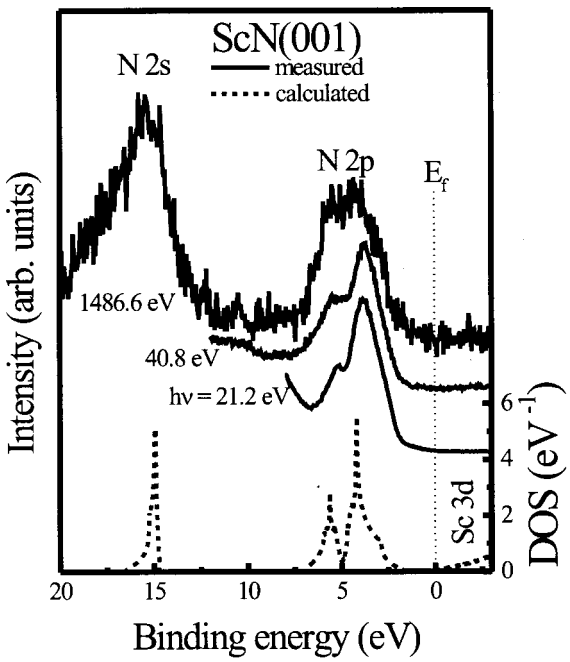

FIG. 5. *In situ* x-ray and ultraviolet valence band photoelectron spectra from ScN(001) layers compared with EXX DOS calculations.

tently higher throughout the entire measured region. These differences, again, are likely to be due to the higher quality of the ScN layers used in the present experiments.

Figure 4(b) is a plot of the complex dielectric function we obtain from the EXX density-functional calculations with $h\nu$ between 0 and 6 eV. The imaginary part ε_2 was obtained from the expression

$$\varepsilon_2(\omega)=\frac{4\pi^2e^2\hbar^2}{3m^2\Omega\omega^2}\sum_{vc\mathbf{k}}|\langle v\mathbf{k}|\mathbf{p}|c\mathbf{k}\rangle|^2\delta(\hbar\omega-\varepsilon_{c\mathbf{k}}+\varepsilon_{v\mathbf{k}}), \tag{6}$$

and the real part from a subsequent Kramers–Kronig transformation. We have neglected exchange-correlation, local-field, and nonlocal pseudopotential effects in Eq. (6). The **k** summation contains 328 **k** points in the irreducible wedge of the Brillouin zone. The calculated ε_2 value is zero up to 2.86 eV, the onset for interband transitions at the X point. ε_2 increases sharply to a peak at 3.2 eV, with a larger second peak at 4.8 eV. The real part of the dielectric function exhibits a peak at 3.0 eV, after which it decreases slowly at first ($3.5<h\nu<4.7$ eV) and then faster near the resonance at 4.8 eV. These results are in agreement with experiment, as discussed in the next section.

Figure 5 shows calculated ScN DOS together with *in-situ* valence-band photoelectron spectra obtained from ScN(001) layers. XPS and UPS spectra were acquired along the $\langle 001\rangle$ growth direction. However, the detector has a large angular acceptance and thus counts photoelectrons from throughout k space. Thus, the resulting measurement corresponds essentially to the total DOS.

The UPS spectra in Fig. 5 exhibit a double peak feature which is associated with the N $2p$ bands at binding energies between 2 and 7 eV. The peaks are centered at 3.8 and 5.2 eV. The increased intensity above 7 eV in the He I spectrum is due to multiply-scattered low-kinetic-energy electrons. XPS features are broadened and noisier than in the UPS spectra due to a lower energy resolution and a lower photoelectron cross section, respectively. The N $2p$ bands appear in the XPS spectrum as one broad feature between 2 and 7 eV while the N $2s$ peak occurs at $\simeq$15.3 eV. The small feature at 10.4 eV is associated with a partial monolayer of surface oxygen adsorbed during the 1.5 h XPS experiment. This peak increases in size when the sample is left in the UHV analysis chamber for 24 h.

The calculated total DOS per eV per unit cell (Fig. 5) was obtained based upon the same 328 special k points used to obtain the dielectric function. The Fermi energy E_f was arbitrarily set to the bottom of the conduction band. Peaks associated with the N $2p$ bands are at 4.2 and 5.6 eV while the N $2s$ peak occurs at a binding energy of 14.9 eV. The DOS above the Fermi level, associated with Sc $3d$ conduction bands, increases slowly and approximately linearly with energy from E_f up to -5 eV (binding energy) with pronounced peaks at -6.5 and -7.1 eV (not shown).

Figure 5 shows that the calculated DOS is in good agreement with the experimental data. The broadening observed in the photoelectron spectra is due to the finite wavelength spread of the photon source and the resolution of the electron detector. To account for this, the calculated DOS spectrum has been convoluted with Gaussian curves of width w. Using $w=0.8$ eV yields a curve (not shown) of essentially identical shape to that of the He I UPS spectrum. The binding energies of the calculated N $2p$ peaks are reduced by 0.1 eV, to 4.1 and 5.5 eV, due to the asymmetry in the DOS peak shapes. Convolving the N $2s$ peak with a Gaussian of $w=1.0$ eV to reproduce the experimental broadening yields a curve very similar to that of the XPS spectrum. The peak occurs at 15.1 eV, 0.2 eV above the originally calculated DOS and close to the XPS peak at $\simeq$15.3 eV.

V. DISCUSSION

The electronic structure of ScN near the Fermi level is composed of the N $2s$ and $2p$ valence bands and the Sc $3d$ conduction bands. While there is a qualitative resemblance between our EXX calculated band structure (Fig. 2) and earlier calculations employing the LDA or the $X\alpha$ approximation,[1,3] there are major differences. The EXX method predicts that ScN is a semiconductor with an indirect Γ to X bandgap of 1.6 eV. LDA and $X\alpha$ results predict a semimetal with band overlaps of 0.21 eV (Ref. 3) and 0.01 eV (Ref. 1), respectively. The Γ and X-point direct gaps are also much larger in EXX than in LDA. The smallest direct gap at the X point is 2.9 and 0.8 eV for EXX and LDA, respectively. The gaps at the Γ point are 4.7 and 5.1 eV in EXX and 2.7 and 3.9 eV in LDA. These large differences in gap energies are a consequence of the repulsive self-interaction present in LDA, which is stronger for the more localized valence electrons and raises their energy with respect to the more delocalized conduction electrons resulting in LDA underestimating the gap.

The absorption spectrum presented in Fig. 3 supports our calculated ScN band structure. The sharp absorption increase near 2.4 eV indicates the onset of direct interband transitions, corresponding to the lowest direct gap at the *X* point. This conclusion is opposite to that of Travaglini *et al.*[17] who, based upon the high absorption they measured below 2 eV, concluded that the LDA band structure calculations are correct. They found an absorption peak at 0.8 eV (Fig. 3), which they related to the direct interband transition at the *X* point while they associated the strong absorption near 2.6 eV to the direct transition at the Γ point. Another interpretation was provided by Dismukes *et al.*[11] who concluded that ScN is a wide band-gap semiconductor. They related the absorption onset they observed above 2 eV to the fundamental gap and neglected the possibility of a smaller indirect gap. Our results clearly show, however, that the observed absorption edge at 2.4 eV is not associated with either a direct transition at the Γ point or with the fundamental gap. Rather, it corresponds to the lowest direct transition at the *X* point, while the fundamental gap is indirect.

The good agreement between our optical measurements and EXX calculations is evident when comparing the dielectric function $\varepsilon=\varepsilon_1+i\varepsilon_2$ obtained from ellipsometry experiments with the $\varepsilon(h\nu)$ spectra obtained from EXX band structure calculations (Fig. 4). ε_1 exhibits a maximum due to the onset of interband transitions at 2.4 and 3.0 eV in experiment and calculation, respectively. ε_2 is small at $h\nu<2$ eV in both experimental and calculational results, consistent with the absence of direct interband transitions over this energy range. Resonance peaks are observed at 2.7 and 3.8 eV in the experiment and at 3.2 and 4.8 eV in the calculation. The two peaks in the imaginary part of the dielectric function correspond to high joint densities-of-states around the *X* and Γ points, respectively.

The experimental ε_1 and ε_2 spectra indicate, in agreement with the absorption data in Fig. 3, that the onset for direct transitions between valence and conduction bands occurs at 2.4 eV, 0.5 eV below the calculated transition energy. The higher direct transition at the Γ point is 1.0 eV below the calculated value. These deviations correspond to only $\simeq$20% of the measured values, which is a significant improvement over LDA calculations, which predict, for example, the direct gap energy at the *X* point to be 0.8 eV, a factor of 3 below the experimental value of 2.4 eV.

The EXX-calculated DOS also exhibits good agreement with valence band photoelectron spectra, as shown in Fig. 5. The binding energy of the calculated double peak feature related to the N $2p$ bands is however, after correction to account for experimental broadening, 0.3 eV larger than measured by UPS. This is a relatively small difference and can be explained within the uncertainty of the EXX calculation (for further details, see Ref. 21). In fact, the calculated N $2p$ DOS agrees perfectly with experiment if E_f in the calculation is reduced by 0.3 eV. This indicates that the bottom of the conduction band is 0.3 eV lower in energy than calculated and we therefore obtain a value for the fundamental indirect gap of $\simeq$1.3 eV, 0.3 eV below the calculated 1.6 eV, which corresponds again to an $\simeq$20% overestimation of the band gap by EXX, consistent with our optical analysis.

The experimental determination of the gap energies also contains some uncertainty which is primarily due to the presence of conduction electrons in our ScN layers with a carrier density of $\simeq 5\times10^{20}\,\mathrm{cm}^{-3}$ as estimated from the free carrier contribution in the optical transmission and reflection spectra. The free carriers are attributed to N vacancies which act as donors similar to anion vacancies in GaN[34,35] and also disturb the periodic potential of the crystal, leading to a band-edge tail as commonly observed in heavily-doped semiconductors.[28] This tail is pronounced and can be clearly observed when comparing the onset of interband transitions in the experimental ε_2 spectra [2.3 eV, Fig. 4(a)] with the calculation [2.8 eV, Fig. 4(b)]. The relatively large carrier density causes a decrease ($<$0.1 eV) in the observed bandgap due to the exchange term in the electron–electron interaction.[36] At the same time, however, the conduction electrons also increase the apparent bandgap due to the Moss–Burstein shift.[28] The size of this shift can be estimated from the carrier density by integrating the EXX DOS. This procedure yields a value of 0.25 eV, the largest contribution to our total uncertainty in bandgap energies which we estimate to be 0.3 eV, including the 0.05 eV uncertainty from the measurement.

Combining the results from the UPS valence band spectroscopy, the EXX calculated DOS, and the above considerations, we conclude that ScN is a semiconductor with an indirect $\Gamma-X$ band gap of 1.3 ± 0.3 eV. The combination of optical analysis and band-structure calculations show that the smallest direct gap is at the *X* point and has a value of 2.4 ±0.3 eV.

VI. SUMMARY AND CONCLUSIONS

We have employed both experimental and *ab initio* computational methods to resolve the debate over whether ScN is a semiconductor or a semimetal, thus whether there is a gap between the N $2p$ and Sc $3d$ bands. ScN layers, 40 to 518 nm thick, were grown at 750 °C on MgO(001) and at 800 °C on 220-nm-thick epitaxial TiN(001) layers on MgO(001) by ultrahigh vacuum reactive magnetron sputter deposition in pure N_2 discharges. The films are stoichiometric with N/Sc ratios, determined by Rutherford backscattering spectroscopy and x-ray photoelectron spectroscopy, of 1.00 ± 0.02. The combination of x-ray diffraction ω–2θ with ω rocking curves and pole figures were used to show that the layers were single crystals which grow with a cube-on-cube epitaxial relationship: $(001)_{\mathrm{ScN}}\|(001)_{\mathrm{TiN}}\|(001)_{\mathrm{MgO}}$ and $[100]_{\mathrm{ScN}}\|[100]_{\mathrm{TiN}}\|[100]_{\mathrm{MgO}}$.

The high quality of the ScN layers used in this investigation was also attested to by the low optical absorption below the onset for direct transitions. α in this region was measured to be $\simeq 6\times10^3\,\mathrm{cm}^{-1}$, two to ten times lower than earlier experimental reports.[11,17] *In-situ* x-ray and ultraviolet valence band photoelectron spectroscopies were used to determine the DOS below the Fermi level. The measured DOS exhibits peaks at 3.8 and 5.2 eV arising from the N $2p$ bands and at 15.3 eV due to the N $2s$ bands. The complex dielectric function $\varepsilon=\varepsilon_1+i\varepsilon_2$ was obtained from spectroscopic ellipsometry experiments. ε_2 has two main features, correspond-

ing to direct transitions near the X and Γ points, at photon energies of 2.7 and 3.8 eV, respectively.

The ScN band structure was calculated using an exact-exchange Kohn–Sham approach. It predicts an indirect gap from the valence band at the Γ point to the conduction band at the X point of 1.6 eV and shows, in contradiction to earlier calculations based on the LDA or the $X\alpha$ approximation[1,3] but consistent with our experimental results, that ScN is a semiconductor. The calculated ScN DOS and complex dielectric function are in good agreement with our valence-band photoelectron spectra and measured optical properties, respectively. A careful comparison of the calculated data with experiments indicates that both the optically-measured direct bandgap at the X point and the fundamental indirect gap determined by photoelectron spectroscopy are $\simeq$20% overestimated by the EXX calculation and that ScN has an indirect Γ to X bandgap of 1.3 ± 0.3 eV.

ACKNOWLEDGMENTS

This work was supported by the U.S. Department of Energy, Division of Materials Science, under Grant No. DEFG0296ER45439 through the University of Illinois Frederick Seitz Materials Research Laboratory. We also appreciate the use of the facilities of the MRL Center for Microanalysis of Materials, which is partially supported by U.S. DOE, at the University of Illinois. M. Städele was supported by the U.S. Office of Naval Research and K. Järrendahl by the Swedish Foundation for International Cooperation in Research and Higher Education (STINT). P.D. was partially supported by the Fonds pour la formation de chercheurs et l'aide à la recherche du Québec (Canada). We thank W.R.L. Lambrecht and Hans Arwin for useful discussions and are indebted to J. A. Majewski and P. Vogl for providing useful subroutines.

APPENDIX

In ellipsometry, the change in polarization state of reflected light from the sample is measured and expressed in the form of the complex reflection ratio. If the measured sample can be treated as a bulk substrate with a perfectly flat and clean surface, the reflection ratio can be expressed as[37]

$$\frac{r_p}{r_s} = \tan\psi e^{i\Delta} \tag{A1}$$

where r_p and r_s are the Fresnel reflection coefficients for the components parallel (p) and perpendicular (s) to the plane of incidence, respectively. Written in polar form, the complex ratio is described by the two parameters Ψ and Δ (the ellipsometric angles), where $\tan\Psi$ and Δ are the amplitude ratio and the phase difference between the p and s components, respectively. The real and imaginary parts of the complex dielectric function $\varepsilon = \varepsilon_1 + i\varepsilon_2$ are obtained by direct inversion from the measured ψ and Δ values. If the sample consists of a substrate covered by one or more layers, the measured reflection ratio is written as

$$\frac{R_p}{R_s} = \tan\psi e^{i\Delta}, \tag{A2}$$

where the reflection coefficients R_p and R_s are functions of the Fresnel reflection coefficients for the interfaces and also of the film thicknesses.[37] In this case, the inversion from ψ and Δ gives the pseudodielectric function $\langle\varepsilon\rangle = \langle\varepsilon_1\rangle + i\langle\varepsilon_2\rangle$. The real dielectric function (and also structural information such as layer thickness and surface roughness) of the films must then be obtained via optical modeling.

It is often a challenge to find unique solutions if more than two parameters are unknown. In the present case, this problem was resolved by determining the complex dielectric function of the ScN films using multiple sample analysis.[31,32] In this method, data from multiple angles of incidence and from two or more samples with different film thicknesses, are analyzed simultaneously. This approach provides unique solutions for both the dielectric function of the films and for the film thicknesses.

[1] A. Neckel, P. Rastl, R. Eibler, P. Weinberger, and K. Schwarz, J. Phys. C **9**, 579 (1976).
[2] R. Eibler, M. Dorrer, and A. Neckel, Theor. Chim. Acta **63**, 133 (1983).
[3] R. Monnier, J. Rhyner, T. M. Rice, and D. D. Koelling, Phys. Rev. B **31**, 5554 (1985).
[4] K. Schwarz, CRC Crit. Rev. Solid State Mater. Sci. **13**, 211 (1987).
[5] R. M. Dreizler and E. K. U. Gross, *Density Functional Theory* (Springer, Berlin, 1990).
[6] L. I. Johansson, Surf. Sci. Rep. **21**, 177 (1995).
[7] L. I. Johansson, A. Callenas, P. M. Stefan, A. N. Christensen, and K. Schwarz, Phys. Rev. B **24**, 1883 (1981).
[8] N. Sclar, J. Appl. Phys. **33**, 2999 (1962).
[9] N. Sclar, J. Appl. Phys. **35**, 1534 (1964).
[10] J. P. Dismukes, W. M. Yim, J. J. Tietjen, and R. E. Novak, RCA Rev. **31**, 680 (1970).
[11] J. P. Dismukes, W. M. Yim, and V. S. Ban, J. Cryst. Growth **13/14**, 365 (1972).
[12] G. Harbeke, E. Meier, and J. P. Dismukes, Opt. Commun. **4**, 335 (1972).
[13] E. Kaldis and Ch. Zürcher, Helv. Phys. Acta **47**, 421 (1974).
[14] T. D. Moustakas, R. J. Molnar, and J. P. Dismukes, *Proceedings of the first symposium on III–V Nitride Materials and Processes*, Electrochemical Society Proceedings (Pennington, NJ, 1996), Vol. 96-11, pp. 197–204.
[15] D. Gall, I. Petrov, L. D. Madsen, J.-E. Sundgren, and J. E. Greene, J. Vac. Sci. Technol. A **16**, 2411 (1998).
[16] L. Porte, J. Phys. C **18**, 6701 (1985).
[17] G. Travaglini, F. Marabelli, R. Monnier, E. Kaldis, and P.

Wachter, Phys. Rev. B **34**, 3876 (1986).
[18] D. Gall, I. Petrov, N. Hellgren, L. Hultman, J.-E. Sundgren, and J. E. Greene, J. Appl. Phys. **84**, 6034 (1998).
[19] D. Gall, I. Petrov, P. Desjardins, and J. E. Greene, J. Appl. Phys. **86**, 5524 (1999).
[20] M. Städele, J. A. Majewski, P. Vogl, and A. Görling, Phys. Rev. Lett. **79**, 2089 (1997).
[21] M. Städele, M. Moukara, J. A. Majewski, P. Vogl, and A. Görling, Phys. Rev. B **59**, 10031 (1999).
[22] R. C. Powell, N.-E. Lee, Y.-W. Kim, and J. E. Greene, J. Appl. Phys. **73**, 189 (1993).
[23] W. Kohn and L. J. Sham, Phys. Rev. **140**, A1133 (1965).
[24] M. Moukara, M. Städele, J. A. Majewski, A. Görling, and P. Vogl, J. Phys. Condens. Matter **12**, 6783 (2000).
[25] R. L. Doolittle, Nucl. Instrum. Methods Phys. Res. B **15**, 344 (1985).
[26] J. F. Moulder, W. F. Stichle, P. E. Sobol, and K. D. Bomben, *Handbook of X-ray Photoelectron Spectroscopy*, edited by J. Chastain and R. C. King Jr. (Physical Electronics, Inc., Eden Prairie USA, 1995).
[27] A. Guinier, *X-ray Diffraction in Crystals, Imperfect Crystals, and Amorphous Bodies* (Freeman, San Francisco, 1963), p. 124.
[28] B. I. Shklovskii, A. L. Efros, *Electronic Properties of Doped Semiconductors* (Springer, Berlin, 1984), p. 287.
[29] D. E. Aspnes, J. B. Theeten, and F. Hottier, Phys. Rev. B **20**, 3292 (1979).
[30] D. E. Aspnes, *Handbook of Optical Constants of Solids*, Ed. E. D. Palik (Academic Press, Orlando, 1985), Ch. 5.
[31] W. A. McGahan, B. Johs, and J. A. Woollam, Thin Solid Films **234**, 443 (1993).
[32] K. Järrendahl and H. Arwin, Thin Solid Films **313–314**, 114 (1998).
[33] F. Wooten, *Optical Properties of Solids* (Academic Press, New York, 1972), p. 46.
[34] W. Kim, A. E. Botchkarev, A. Salvador, G. Popovici, H. Tang, and H. Morkoç, J. Appl. Phys. **82**, 219 (1997).
[35] S. J. Pearton, J. C. Zolper, R. J. Shul, and F. Ren, J. Appl. Phys. **86**, 1 (1999).
[36] V. I. Fistul, *Heavily Doped Semiconductors* (Plenum Press, New York, 1969), p. 33.
[37] R. M. A. Azzam and N. M. Bashara, *Ellipsometry and Polarized Light* (North-Holland, Amsterdam, 1977).